Physica D 325 (2016) 63–73

Contents lists available at ScienceDirect

Physica D

journal homepage: www.elsevier.com/locate/physd

A numerical method for computing initial conditions of Lagrangian invariant tori using the frequency map☆

Alejandro Luque [a,*], Jordi Villanueva [b]

[a] Instituto de Ciencias Matemáticas, Consejo Superior de Investigaciones Científicas, C. Nicolás Cabrera 13-15, 28049 Madrid, Spain
[b] Departament de Matemàtica Aplicada I, Universitat Politècnica de Catalunya, Av. Diagonal 647, 08028 Barcelona, Spain

HIGHLIGHTS

- A method to compute initial conditions on Lagrangian invariant tori is proposed.
- Initial condition are found by imposing suitable conditions on the frequency map.
- The basic tool is an averaging-extrapolation strategy to perform frequency analysis.
- The proposed approach performs with high accuracy at a moderate computational cost.

ARTICLE INFO

Article history:
Received 9 June 2015
Received in revised form
19 February 2016
Accepted 21 February 2016
Available online 10 March 2016
Communicated by H.A. Dijkstra

Keywords:
Quasi-periodic Lagrangian tori
Hamiltonian systems
Symplectic maps
Derivatives of frequencies

ABSTRACT

We present a numerical method for computing initial conditions of Lagrangian quasi-periodic invariant tori of Hamiltonian systems and symplectic maps. Such initial conditions are found by solving, using the Newton method, a nonlinear system obtained by imposing suitable conditions on the frequency map. The basic tool is a newly developed methodology to perform the frequency analysis of a discrete quasi-periodic signal, allowing to compute frequencies and their derivatives with respect to parameters. Roughly speaking, this method consists in computing suitable weighted averages of the iterates of the signal and using the Richardson extrapolation method. The proposed approach performs with high accuracy at a moderate computational cost. We illustrate the method by considering a discrete FPU model and the vicinity of the point L_4 in a RTBP.

1. Introduction

One of the most remarkable features of Hamiltonian systems and symplectic maps is the huge abundance of quasi-periodic solutions. We refer the interested reader to [1,2], and references therein, for a wide picture of quasi-periodicity in dynamical systems. A typical way to introduce quasi-periodic solutions is to consider perturbations of integrable systems. The phase space of an integrable Hamiltonian is filled up by *Lagrangian invariant tori carrying quasi-periodic motion* (LIT). The KAM theorem states that most of the LITs of the integrable system, in the sense of the Lebesgue measure, survive to small Hamiltonian perturbations. LITs are also abundant far from integrability, as there are many mechanisms to generate them.

As invariant tori are a fundamental class of stable solutions, computing them is a very relevant problem in the numerical analysis of dynamical systems, and a wide set of algorithms has been developed for this purpose. We summarize some methods for computing LITs and we refer the reader to [3,4] for a more detailed discussion of the bibliography. LITs have been approximated using methods based on canonical transformations (e.g. implementation of KAM proofs [5] or normal forms around an invariant object [6,7]) or using the Lindstedt–Poincaré method [6,8]. Another approach, valid far from integrability, is to compute a parameterization of the LIT as a solution of an invariance equation. This functional equation can be approximated by a finite dimensional one, either by discretizing the functional (e.g. [9,4]) or by truncating the Fourier series of the parameterization (e.g. [10–12]). Some recent works (e.g. [3,13]) solve the invariance equation by methods based on the

☆ This work has been supported by the Spanish MINECO-FEDER Grants MTM2015-65715-P, MTM2012-32541 and the Catalan Grants 2014SGR504 and 2014SGR1145. Moreover, A. L. is supported by a postdoctoral position in the ERC Starting Grant 335079 and partially supported by the ICMAT–Severo Ochoa grant SEV-2015-0554 (MINECO).

* Corresponding author.
E-mail addresses: luque@icmat.es (A. Luque), jordi.villanueva@upc.edu (J. Villanueva).

http://dx.doi.org/10.1016/j.physd.2016.02.014
0167-2789/

parameterization KAM result in [14]. Finally, invariant curves of maps have been computed by interpolating the dynamics [15,8]. This last approach is the closest to our construction, in the sense that it also attempts to compute the curve by finding a single point of it.

In this paper we compute initial conditions of LITs with prefixed frequencies. To this end we assume that LITs can be locally labeled by the frequency vector (e.g under the Kolmogorov non-degeneracy condition). We can identify a point on the LIT by equating the frequency map to the selected frequencies. This leads to a nonlinear system of equations with dimension given by the number of degrees of freedom. If we can evaluate the frequency map at any point, as well as its derivatives, then this system can be solved by the Newton method.

To compute frequencies and their derivatives at a given point, we use an averaging-extrapolation method applied to a sample of points of the corresponding orbit. This approach, that was introduced in [16] to compute rotation numbers of circle maps, allows computing the frequencies with an error of $\mathcal{O}(1/N^{p+1})$, where p is the averaging order and N the length of the sample. Subsequently, this method was extended to compute derivatives of the rotation number [17], to compute quasi-periodic invariant curves of symplectic maps [18] and to perform the frequency analysis of an arbitrary quasi-periodic signal [19]. Notice that there are other noteworthy methods for the quasi-periodic frequency analysis (e.g. [20,21]) that could be used also to evaluate the frequency map.

Our approach does not require the system to be nearly-integrable nor to be written in a specific set of coordinates. We do not approximate the LIT using Fourier series and we do not solve any system of large dimension. Hence, the method is not limited by memory storage (e.g. the number of Fourier coefficients needed to approximate a LIT rapidly increases with the dimension). However, in this way we do not get the parameterization of the LIT (it has to be computed a posteriori, if required).

2. Description of the methods

In this section we introduce the formal approach to obtain initial conditions on a LIT using the frequency map. Then we outline the basic ideas of the averaging-extrapolation methods that we use to compute the frequency map, its derivatives, and the Fourier coefficients of the parameterization of the LIT. We sketch the basic formulas and parameters of the method, and refer the reader to [17,19,16] for implementation details.

2.1. Setting of the problem and formal approach

We describe the use of the frequency map to obtain initial conditions on a LIT with prefixed frequencies. This approach works both for Hamiltonians and symplectic maps, assuming large enough regularity. However, to simplify the presentation, we concentrate on analytic Hamiltonians. Let $h : U \subset \mathbb{R}^{2r} \to \mathbb{R}$ be an analytic Hamiltonian with r degrees of freedom. We suppose $\mathcal{T}$ is a LIT of dimension r of h, with Diophantine frequency vector $\omega \in \mathbb{R}^r$:

$$|\langle k, \omega\rangle| \geq \frac{C}{|k|_1^{\tau}}, \quad \forall k \in \mathbb{Z}^r \setminus \{0\},\ |k|_1 = |k_1| + \cdots + |k_r|, \tag{1}$$

for $C, \tau > 0$. This means that there is a parameterization of $\mathcal{T}$ given by a real analytic embedding φ such that:

$$\varphi : \mathbb{T}^r \to \mathbb{R}^{2r}, \qquad \mathcal{T} = \varphi(\mathbb{T}^r), \qquad L_\omega \varphi(\theta) = J\nabla h(\varphi(\theta)), \tag{2}$$

where $\mathbb{T}^r = (\mathbb{R}/2\pi\mathbb{Z})^r$, $L_\omega = \sum_{j=1}^r \omega_j \partial_{\theta_j}$, and J is the matrix of the symplectic form. We refer to (2) as the condition of invariance of φ.

The KAM theorem ensures that, under suitable non-degeneracy conditions, there are plenty of real analytic LITs around $\mathcal{T}$ that are invariant by h, with frequencies moving with the torus. These LITs fill up a Cantor-like set $U^* \subset U$ of large Lebesgue measure. Indeed, the Lebesgue measure of the portion of the phase space not filled up by LITs is exponentially small in the distance to $\mathcal{T}$ (e.g. [22]). Although U^* has empty interior, these LITs are organized as a Whitney-$\mathcal{C}^\infty$ Cantor family (e.g. [1]). Hence, there is a Cantor-like set $\mathcal{K} \subset \mathbb{R}^r$ and functions $\Omega : \mathcal{K} \to \mathbb{R}^r$ and $\Psi : \mathbb{T}^r \times \mathcal{K} \to \mathbb{R}^{2r}$ such that $\theta \mapsto \Psi(\theta, I)$ is an analytic parameterization of a LIT with frequency vector $\Omega(I)$. We normalize them so that $\varphi(\cdot) = \Psi(\cdot, 0)$ and $\omega = \Omega(0)$. Both, Ω and Ψ, are Whitney-$\mathcal{C}^\infty$ functions that can be extended to $\mathcal{C}^\infty$-functions on open sets around $I = 0$ and $(\theta, I) \in \mathbb{T}^r \times \{0\}$, respectively. The (Kolmogorov) non-degeneracy condition at $\mathcal{T}$ is $\det(D\Omega(0)) \neq 0$. We introduce the frequency map

$$\mathcal{F} : U^* \subset \mathbb{R}^{2r} \to \mathbb{R}^r \tag{3}$$

that assigns to any point of $U^* = \Psi(\mathbb{T}^r \times \mathcal{K})$ the corresponding frequency vector. The value of $\mathcal{F}(x)$ is defined as $\mathcal{F}(x) = \Omega(I_x)$, with $I_x \in \mathcal{K}$ given by the inverse of Ψ. Specifically, $x = \Psi(\theta_x, I_x)$ for some $\theta_x \in \mathbb{T}^r$. Note that the function $\mathcal{F}(x)$ is only properly defined if x belongs to some LIT of the family. However, the Whitney-$\mathcal{C}^\infty$ character of Ω and Ψ implies that $\mathcal{F}$ can be extended to the whole set U as a $\mathcal{C}^\infty$ function of the initial conditions.

We use the information provided by $\mathcal{F}$ and its derivatives to compute an initial condition on $\mathcal{T}$. From the practical viewpoint, we must be far away from low-order resonances. Assume that we have a point $x^{(0)} \in U^*$, close to $\mathcal{T}$, so that we can assign to $x^{(0)}$ a Diophantine frequency vector $\mathcal{F}(x^{(0)})$. We look for a small correction $\Delta x^{(0)} \in \mathbb{R}^{2r}$ in such a way that $x^{(0)} + \Delta x^{(0)}$ is closer to $\mathcal{T}$ than $x^{(0)}$. By the non-degeneracy of $\mathcal{F}$, the condition $x^{(0)} + \Delta x^{(0)} \in \mathcal{T}$ is equivalent to the following r-dimensional nonlinear system of equations:

$$\mathcal{F}(x^{(0)} + \Delta x^{(0)}) = \omega. \tag{4}$$

The linearized system of (4) is given by

$$D\mathcal{F}(x^{(0)})\Delta x^{(0)} = \omega - \mathcal{F}(x^{(0)}), \tag{5}$$

where $D\mathcal{F}(x^{(0)})$ is a $r \times 2r$-matrix of maximum range. We must add appropriate normalization conditions (depending on the context at hand) to secure a single solution of (4). Our customary choice is to set to zero the value of r coordinates of $\Delta x^{(0)}$. Then, we introduce the sequence $x^{(i+1)} = x^{(i)} + \Delta x^{(i)}$ and we expect $\mathcal{F}(x^{(i+1)})$ to take the value ω with an error $\mathcal{O}(|\omega - \mathcal{F}(x^{(i)})|^2)$. This approach can be adapted directly to several contexts: systems depending periodically or quasi-periodically on time, iso-energetic non-degenerate conditions, exact symplectic maps or dependence on external parameters.

To perform a correction of the Newton method, we follow the next basic steps:

- Let $x^{(0)} \in U$ be a point of a LIT close to $\mathcal{T}$, with unknown frequency vector $\widetilde{\omega} \simeq \omega$ that verifies Diophantine properties like (1). We introduce the sequence $\{x_n\}$ defined by $x_n = \phi(nT; x^{(0)})$, where ϕ is the flow of h and T is a sampling time. This sequence carries quasi-periodic motion with frequency vector $\bar{\omega} = T\widetilde{\omega}$. To compute $\{x_n\}$, and its derivatives, we have to integrate numerically the trajectory of $x^{(0)}$ together with the corresponding variational equations. If $x^{(0)}$ belongs to a LIT of an exact symplectic map f, with frequency vector $\widetilde{\omega}$, then the sequence $\{x_n\}$ is directly obtained as $x_n = f^n(x^{(0)})$, and we have $\bar{\omega} = \widetilde{\omega}$.

- From $\{x_n\}$ we set a complex discrete quasi-periodic signal $\{z_n\}$ with the same frequency vector $\bar{\omega}$. If we denote $x_n = (x_n^1, \ldots, x_n^r)$ we can set, for example, $z_n = x_n^1$ or $z_n = x_n^1 + \mathrm{i}x_n^2$. This choice depends on the problem at hand. Using an averaging-extrapolation process (see Section 2.2) we construct a new quasi-periodic signal whose rotation frequency around the origin is a selected component of $\bar{\omega}$. We refer to this process as the unfolding of the signal.
- By projecting the unfolded signal we define a quasi-periodic signal of $\mathbb{T}$. The rotation frequency of the projected signal is computed using averaging and extrapolation (see Section 2.3), in analogous way as it is done in [16] for the rotation number of a map of the circle. Derivatives of the frequencies with respect to initial conditions and parameters are computed by taking formal derivatives on the extrapolation operators.

2.2. Unfolding of the signal

We say that the complex sequence $\{z_n\}_{n\in\mathbb{Z}}$ is a (discrete) quasi-periodic signal with frequency vector $\bar{\omega} \in \mathbb{R}^r$ if there is $\gamma : \mathbb{T}^r \to \mathbb{C}$ such that $z_n = \gamma(n\bar{\omega})$, $\forall n \in \mathbb{Z}$. If we denote the Fourier expansion of γ as

$$\gamma(\theta) = \sum_{k\in\mathbb{Z}^r} \hat{\gamma}_k \mathrm{e}^{\mathrm{i}\langle k,\theta\rangle}, \quad \hat{\gamma}_k = \frac{1}{(2\pi)^r}\int_{\mathbb{T}^r} \gamma(\theta)\mathrm{e}^{-\mathrm{i}\langle k,\theta\rangle} d\theta,$$

then we have the relation

$$z_n = \gamma(n\bar{\omega}) = \sum_{k\in\mathbb{Z}^r} \hat{\gamma}_k \mathrm{e}^{\mathrm{i}n\langle k,\bar{\omega}\rangle}. \tag{6}$$

In this context, we say that $\bar{\omega}$ is a Diophantine frequency vector if there exists $\bar{C}$, $\tau > 0$ such that

$$|\mathrm{e}^{\mathrm{i}\langle k,\bar{\omega}\rangle} - 1| \geq \frac{\bar{C}}{|k|_1^{\tau}}, \quad \forall k \in \mathbb{Z}^r \setminus \{0\}. \tag{7}$$

The conditions in (7) for a discrete quasi-periodic signal are equivalent to say that $(\bar{\omega}, 2\pi) \in \mathbb{R}^{r+1}$ verifies (1) for certain $C > 0$. Note that the fact that $\widetilde{\omega}$ verifies (1) does not imply that $\bar{\omega} = T\widetilde{\omega}$ verifies (7). But, if $\widetilde{\omega}$ is far away from low-order resonances, we expect $\bar{\omega}$ to behaves like (7) for the practical viewpoint. See [19] for details.

Given $\omega_0 \in \mathbb{R}$, we introduce the phase-shifted iterates

$$\mathcal{Z}_n^{(l,\omega_0,0)} = z_{n+l-1}\mathrm{e}^{-\mathrm{i}(n+l-1)\omega_0}, \quad n \geq 1,\ l \geq 1, \tag{8}$$

the recursive sums

$$\mathcal{Z}_n^{(L,\omega_0,p)} = \sum_{l=1}^{L} \mathcal{Z}_n^{(l,\omega_0,p-1)}, \quad n \geq 1,\ L \geq 1,\ p \geq 1, \tag{9}$$

and the averaged sums

$$\hat{\mathcal{Z}}_n^{(L,\omega_0,p)} = \binom{L+p-1}{p}^{-1} \mathcal{Z}_n^{(L,\omega_0,p)}. \tag{10}$$

We undo the phase-shift in order to introduce the sequence

$$\widetilde{\mathcal{Z}}_n^{(L,\omega_0,p)} = \hat{\mathcal{Z}}_n^{(L,\omega_0,p)} \mathrm{e}^{\mathrm{i}n\omega_0}. \tag{11}$$

Then, we use the asymptotic behavior of $\widetilde{\mathcal{Z}}_n^{(L,\omega_0,p)}$ when $L \to \infty$ in order to carry out an extrapolation process. Given the extrapolation parameters p_u, $q_u \in \mathbb{N}$, with $q_u \geq p_u$, we define the sequence

$$z_n^{(2^{q_u},\omega_0,p_u)} = \sum_{j=0}^{p_u-1} c_j^{(p_u-1)} \widetilde{\mathcal{Z}}_n^{(L_j,\omega_0,p_u)}, \quad n \geq 1, \tag{12}$$

where $L_j = 2^{q_u-p_u+j+1}$ and the (extrapolation) coefficients $c_j^{(m)}$ are given by

$$c_j^{(m)} = (-1)^{m-j}\frac{2^{j(j+1)/2}}{\delta(j)\delta(m-j)}, \tag{13}$$
$$\delta(n) = (2^n-1)(2^{n-1}-1)\cdots(2^1-1), \qquad \delta(0) = 1.$$

If $\{z_n\}$ is an analytic signal and $\bar{\omega}$ verifies (7), then $\{z_n^{(2^{q_u},\omega_0,p_u)}\}$ defines a quasi-periodic signal with frequency vector $\bar{\omega}$ given by the analytic function $\gamma^{(2^{q_u},\omega_0,p_u)} : \mathbb{T}^r \to \mathbb{C}$. From Proposition 2.12 in [19], if ω_0 is close enough to a particular component of $\bar{\omega}$, say $\bar{\omega}_1$, (in the sense that $2^{q_u}|\bar{\omega}_1 - \omega_0|$ is fairly small) we have

$$|z_n^{(2^{q_u},\omega_0,p_u)} - \hat{\gamma}_{e_1}^{(2^{q_u},\omega_0,p_u)}\mathrm{e}^{\mathrm{i}n\bar{\omega}_1}| = \mathcal{O}(2^{-p_u q_u}), \quad \forall n \in \mathbb{Z},$$

where $\hat{\gamma}_{e_1}^{(2^{q_u},\omega_0,p_u)}$ is the Fourier coefficient of $\gamma^{(2^{q_u},\omega_0,p_u)}$ associated to $\bar{\omega}_1$. For this reason, we say that the signal associated to (12) gives an unfolding of order p_u of $\{z_n\}_{n\in\mathbb{Z}}$ for the frequency $\bar{\omega}_1$. The construction follows using the Richardson extrapolation method on the explicit expression of the averaged sums (10). Notice that, within the present context, as $\widetilde{\omega} \simeq \omega$, and the frequency vector of the target torus is known, then we can select ω_0 as $T\omega_1$.

In case that we do not have information on the frequencies of the signal, we can use any method of quasi-periodic frequency analysis in order to select a suitable value of ω_0. These methods are based on a refined analysis of a DFT of the signal (e.g. [20,21]). In our context, we observe that the map

$$\omega_0 \mapsto \frac{1}{L}\sum_{m=0}^{L-1} z_m \mathrm{e}^{-m\omega_0\mathrm{i}} = \widetilde{Z}_0^{(L,\omega_0,1)}$$

produces the DFT of the signal $\{z_m\}_{m=0}^{L-1}$ when applied to a sampling of the form $\omega_0 = \frac{2\pi k}{L}$. Then, we refer to [19] for a construction that uses the averaged sums $\widetilde{Z}_0^{(L,\omega_0,p)}$ to improve the information provided by the DFT. Furthermore, it is worth noticing that, using the terminology of *digital signal processing* (DSP), the construction (8)–(11) constitutes a linear band-pass filter, composed of a frequency shift $\omega_0 \to 0$, given by (8), a low-pass filter, given by (9) and (10), and a frequency shift $0 \to \omega_0$, inverse of the first one, given by (11). This band-pass filter attenuates amplitudes for frequencies different from ω_0 and the extrapolation (12) and (13) enhances this attenuation effect. This attenuation produces the unfolding mentioned above. We remark that this filter preserves both the analyticity and frequency vector of the initial signal. If amplitudes for frequencies different from $\bar{\omega}_1 \approx \omega_0$ are sufficiently attenuated relative to the amplitude at $\bar{\omega}_1$, then $\bar{\omega}_1$ becomes the rotation frequency around the origin (i.e, $\bar{\omega}_1/2\pi$ is the average number of turns of the unfolded signal around the origin).

The fact that $\bar{\omega}_1$ is the rotation frequency means that if we consider the projection to $\mathbb{T}$

$$x_n^{(2^{q_u},\omega_1^0,p_u)} = \arg(z_n^{(2^{q_u},\omega_1^0,p_u)}), \tag{14}$$

then we can write

$$x_n^{(2^{q_u},\omega_1^0,p_u)} = n\bar{\omega}_1 + X^{(2^{q_u},\omega_1^0,p_u)}(n\bar{\omega}), \tag{15}$$

where $X^{(2^{q_u},\omega_1^0,p_u)} : \mathbb{T}^r \to \mathbb{R}$ is an analytic function. The expression (15) denotes the lift to $\mathbb{R}$ of the projected signal rather than the signal of $\mathbb{T}$ itself (i.e. the argument must be increased by 2π whenever $z_n^{(L,\omega_1^0,p_u)}$ completes one turn around the origin). In practice, we say that the unfolding of the signal $\{z_n\}$ has succeeded if we can set $\bar{\omega}_1$ as the value of the rotation frequency and if we are able to track the evolution of the argument along the unfolded iterates. Taking values $p_u = 2$ and $q_u = 10$ is enough in most situations. We refer to [19] for efficient recurrences to compute the unfolded signal.

Although we have described the unfolding process corresponding to a particular frequency $\bar{\omega}_1$, in practice we perform this process simultaneously for all the components of $\bar{\omega}$. In this way, we do not need to store in memory the integration sample and we also save several loops in the algorithm.

2.3. Computation of the frequency vector and derivatives

We introduce the recursive sums

$$S_n^{(0)} = x_n^{(2^{q_u},\omega_1^0,p_u)}, \qquad S_n^{(p)} = \sum_{m=1}^{n} S_m^{(p-1)}, \quad n \geq 1,\ p \geq 1, \tag{16}$$

and the averaged sums

$$\widetilde{S}_n^{(p)} = \binom{n+p}{p+1}^{-1} S_n^{(p)}.$$

Given the extrapolation parameters $p_r, q_r \in \mathbb{N}$, with $q_r \geq p_r$, we introduce the operator

$$\Theta^{(p_r,q_r)} = \sum_{j=0}^{p_r} c_j^{(p_r)} \widetilde{S}_{N_j}^{(p_r)}, \tag{17}$$

where $N_j = 2^{q_r-p_r+j}$, and the coefficients $c_j^{(m)}$ are given by (13). If Eq. (15) holds, it turns out that

$$\bar{\omega}_1 = \Theta^{(p_r,q_r)} + \mathcal{O}(2^{-q_r(p_r+1)}).$$

We refer the reader to [19,16] for justifications, details on optimal selection of the parameters p_r and q_r, and complete description of implementation details. We observe that to compute the recursive sums $\{S_{N_j}^{(p_r)}\}_{j=0}^{p_r}$ we only need to store in memory a $(p_r+1)\times(p_r+1)$ matrix array. We do not need to store the iterates of the signal. We also point out the recent work [23] for a similar approach to the computation of rotation frequencies.

Assume that the problem depends (at least $\mathcal{C}^1$) on a parameter α. We observe that the linear structure of the operator $\Theta^{(p_r,q_r)}$ (and of the unfolding procedure of Section 2.2) commutes with the differential operator ∂_α. For this reason, the above method can be directly extended to compute derivatives with respect to parameters. Hence, we can compute approximations of $\partial_\alpha \bar{\omega}_1$ by taking formal derivatives on these operators. Then, we introduce the sums $\partial_\alpha S_{N_j}^{(p_r)}$, associated to $\{\partial_\alpha x_n^{(L,\omega_1^0,p_u)}\}$, using the same recurrences as in (16), and we obtain

$$\partial_\alpha \bar{\omega}_1 = \partial_\alpha \Theta^{(p_r,q_r)} + \mathcal{O}(2^{-q_r p_r}).$$

We refer the reader to [24,17] for an exhaustive discussion and implementation details. If the signal is given through a Hamiltonian flow or a symplectic map, we cannot expect it to be well-defined for every value α, but only for a Cantor set. According to the discussions in Section 2.1, we expect that $\partial_\alpha \bar{\omega}(\alpha)$ is well defined in the sense of Whitney. We remark that the method works for computing higher order derivatives of $\bar{\omega}_1$, but the computations become more difficult when the order increases. Specifically, for a derivative of order d the extrapolation error is controlled by $\mathcal{O}(2^{-q_r(p_r+1-d)})$.

To perform our methodology we have to compute a sample of M points of this signal, as well as its derivatives with respect to initial conditions and parameters. Note that if we unfold the signal using parameter values p_u and q_u and we refine the frequencies using parameter values p_r and q_r, then $M = 2^{q_u} + 2^{q_r} - 1$.

2.4. Computation of the Fourier coefficients

In many applications, we may be interested in computing the parameterization φ of a LIT rather that a single point on it. By computing several Fourier coefficients of φ we obtain an initial guess to use the parameterization method in KAM theory (e.g. [14,3,13]). In turns out that the averaging-extrapolation method can be adapted to deal with this scenario.

Let $\mathcal{T}$ be a LIT with frequency vector ω and assume that we have computed $x^* \in \mathcal{T}$ by solving (4). Let $\varphi : \mathbb{T}^r \to \mathbb{R}^{2r}$ be the parameterization of $\mathcal{T}$, given by (2), such that $\varphi(0) = x^*$ and let $\{\hat{\varphi}_k\}_{k\in\mathbb{Z}^r}$ be the Fourier coefficients of φ. Unfortunately, we cannot obtain $\{\hat{\varphi}_k\}_{k\in\mathbb{Z}^r}$ directly by DFT since we only can evaluate a trajectory on the LIT, and so, we cannot generate the values of φ on an equispaced grid of points on $\mathbb{T}^r$. As this trajectory is dense on $\mathcal{T}$, we have the option of using interpolation to get approximations to the values of φ on the grid, but the error of interpolation can be large when r increases. Next, we explain how we can get Fourier coefficients by averaging an extrapolation.

We consider the signal $\{x_n\}$, with $x_n = \phi(nT; x^*)$, where ϕ is the flow of h and T is the sampling time. Then, the frequency vector of this signal is $T\omega$. The computed values satisfy $x_n = \varphi(nT\omega)$. Hence, the corresponding points of $\mathbb{T}^r$ are not equispaced, but distributed according to the translational dynamics by $T\omega$. Given a fixed $k \in \mathbb{Z}^r$, the expression $x_n^{(k)} = x_n e^{-inT\langle k,\omega\rangle}$ defines a discrete quasi-periodic signal of $\mathbb{C}^{2r}$ with frequency vector $T\omega$ and average $\hat{\varphi}_k$. We introduce $S_n^{(0)}(k) = x_n^{(k)}$, we compute the recursive sums $S_n^{(p)}(k)$ using Eq. (16), and we introduce the averages

$$\widetilde{S}_n^{(p)}(k) = \binom{n+p-1}{p}^{-1} S_n^{(p)}(k).$$

Given $p_f, q_f \in \mathbb{N}$, with $q_f \geq p_f$, we define

$$\Gamma_k^{(p_f,q_f)} = \sum_{j=0}^{p_f-1} c_j^{(p_f-1)} \widetilde{S}_{N_j}^{(p_f)}(k), \tag{18}$$

where $N_j = 2^{q_f-p_f+j+1}$ and the coefficients $c_j^{(p_f-1)}$ are given by (13). Then, it turns out that

$$\hat{\gamma}_k = \Gamma_k^{(p_f,q_f)} + \mathcal{O}(2^{-q_f p_f}).$$

We refer the reader to [19] for a complete description of implementation details.

In practice, it may be interesting to take $p_f = p_r + 1$ and $q_f = q_r$. Then the operators in (17) and (18) are applied to the same sample of $N = 2^{q_r}$ iterates. Using the operator (18), we can compute a selected set of Fourier coefficients, with high precision, independently of the other ones. Among the drawbacks of this approach, we stress the fact that we miss the orthogonality properties of the DFT. This lack of orthogonality increases the perturbative effect of the dominant Fourier coefficients when computing $\hat{\varphi}_k$ for large values of $|k|$. For this reason, it may be a good idea to start by computing the dominant part of φ. If we subtract this from the signal, then we magnify the contribution of the high order frequencies (this is a typical approach when performing a quasi-periodic frequency analysis with methods based on DFT, e.g. [20,21]). We remark again that an interesting possibility is to compute a rough approximation to φ, and then to refine it by means of a parameterization method. An analogous strategy is useful if we want a point on $\mathcal{T}$, but "far away" from x^* (e.g., the intersection of $\mathcal{T}$ with a certain transverse manifold). We can use a rough approximation to φ to locate a point close to $\mathcal{T}$ verifying also the desired properties. Then, we can refine this point by the methodology of this paper.

Finally, we can use the extrapolation operator (18) to validate the computation of the frequency in Section 2.3. Assume that we want to check whether $\Theta^{(p_r,q_r)}$ provides a true approximation to $\bar{\omega}_1$. We can proceed by computing the Fourier coefficient $\hat{\gamma}_{e_1}$ associated to this frequency, using $\Theta^{(p_r,q_r)}$ to compute $x_n^{(e_1)}$. If $\Theta^{(p_r,q_r)}$ approximates a frequency of $\{z_n\}$, then $\hat{\gamma}_{e_1} \neq 0$. Accordingly, if we numerically obtain that $\hat{\gamma}_{e_1} = 0$, then $\Theta^{(p_r,q_r)}$ is not an approximation to $\bar{\omega}_1$. In this case we must improve the unfolding process by taking a larger value of L to define each unfolded iterate or by looking for a better approximation to $\bar{\omega}_1$ than ω_1^0.

3. Numerical examples

We consider two different examples in order to enhance the main features and limitations of the presented methods. In Section 3.1 we study a simple model that describes a coupled chain of anharmonic oscillators. The main reason for considering this discrete-time system is because dealing with this symplectic map we can easily compute a large number of iterates with a simple implementation and fast computational time. In Section 3.2 we compute some families of LITs in a Restricted Three Body Problem. We consider different situations involving the planar and the spatial cases, and also the circular and the elliptic cases.

3.1. A model of coupled anharmonic oscillators

The considered FPU model is a discretization of a canonical model describing r anharmonic oscillators with a local coupling that has been extensively studied in the literature (e.g. [25,26]) after the pioneering work of Fermi, Pasta and Ulam in [27]. We consider $x \in \mathbb{T}^r$ and $y \in \mathbb{R}^r$, where we set $\mathbb{T} = \mathbb{R}/\mathbb{Z}$ in order to follow the common convention in the literature. Then, the dynamics is given by the exact symplectic map $(\bar{x}, \bar{y}) = F(x, y)$ defined as

$$\begin{aligned} \bar{x}_i &= x_i + \bar{y}_i, \\ \bar{y}_i &= y_i - \frac{\alpha_i}{2\pi}\sin(2\pi x_i) + \frac{\beta}{2\pi}\sin(2\pi(x_{i+1} - x_i)) \\ &\quad - \frac{\beta}{2\pi}\sin(2\pi(x_i - x_{i-1})), \end{aligned} \tag{19}$$

for $i = 1, \ldots, r$, where we identify $x_0 = x_r$ and $x_{r+1} = x_1$. The parameters $\{\alpha_i\}_{i=1}^r$ are associated to the anharmonic oscillators and β measures the coupling between the oscillators. Notice that each iterate is obtained just by evaluating $2r$ times the sinus function and performing few elemental operations. Hence, we can compute a huge number of iterates of the map (19), as well as its derivatives, up to a high accuracy but with a moderate computational cost. To exploit this fact, we perform computations using an arithmetic of 32 decimal digits.

In this example, we use $p_u = 2$ and $q_u = 10$ for the unfolding procedure and we use $p_r = 8$ and $q_r \leq 20$ for the computation of the frequencies and its derivatives. We compute approximations to the frequencies using 2^{q_r} unfolded iterates, increasing the value of q_r from 8 to 20. We stop when the difference between two consecutive approximations is smaller than a prefixed tolerance. Approximations of the derivatives of the frequencies are computed by using the same number of iterates needed to validate the frequencies. The tolerance for the computation of the frequencies and the tolerance for the Newton method are selected according to each particular situation.

For $\beta = 0$ the model (19) turns out to be the product of r uncoupled standard maps [28] of the form

$$(x, y) \mapsto \left(\bar{x} = x + \bar{y},\ \bar{y} = y - \frac{\alpha}{2\pi}\sin(2\pi x)\right). \tag{20}$$

For $\alpha = 0$, the circles $\mathbb{T} \times \{\omega\}$ are invariant and with rotation number ω. If ω is Diophantine and $|\alpha|$ is small enough, the map (20) has an invariant curve with rotation number ω. Since (20) is a twist map, the projection of this invariant curve onto $\mathbb{T}$ defines a circle map with rotation number ω. This fact allows performing the numerical continuation with respect to α of an initial condition on this curve, without needing to carry out the unfolding procedure. Hence, we obtain an analytic curve $y^0(\alpha)$ so that $(0, y^0(\alpha))$ belongs to an invariant curve of (20) with rotation number ω. We refer the reader to [17,16] for details on this specific continuation. This curve is used later on to initialize the computation of LITs of (19) for higher number of coupled oscillators.

For $r = 2$ the model (19) defines a Froeschlé-like map $F_{\alpha_1,\alpha_2,\beta}$. The Froeschlé map [29] has been used as a model to understand instability channels. In this case, we can only ensure that the direct projection of the iterates onto the angular variables $(x_1, x_2) \in \mathbb{T}^2$ is well-posed if $|\alpha|, |\beta| \ll 1$. For general values of α and β, we should use the unfolding procedure. We fix a Diophantine rotation vector $\omega^0 = (\omega_1^0, \omega_2^0)$ (i.e., the frequency vector is $2\pi\omega^0$) and we consider the LIT of $F_{\alpha_1,\alpha_2,\beta}$, for $\beta = 0$, defined as the product of the invariant curves of (20) for $\alpha = \alpha_1$ and $\alpha = \alpha_2$, with rotation number ω_1^0 and ω_2^0, respectively. Then, we fix the values α_1 and α_2, and we perform the numerical continuation with respect to β of the LIT of $F_{\alpha_1,\alpha_2,\beta}$ with rotation frequency ω^0. To apply the methods of Section 2, we consider initial conditions of the form $(x_1^0, x_2^0, y_1^0, y_2^0)$, with $x_1^0 = 0$, and $x_2^0 = 0$, and we deal with the complex signal

$$z_n = (1 + y_1^n)e^{2\pi i x_1^n} + (1 + y_2^n)e^{2\pi i x_2^n},$$

that is defined in terms of the orbit $(x_1^n, x_2^n, y_1^n, y_2^n) = F_{\alpha_1,\alpha_2,\beta}^n(0, 0, y_1^0, y_2^0)$. Abusing notation, we denote by ω_1 and ω_2 the components of the frequency map of $F_{\alpha_1,\alpha_2,\beta}$. Since the values of α_1 and α_2 are fixed, and we select initial conditions with $x_1^0 = 0$ and $x_2^0 = 0$, we have to evaluate the derivatives

$$\frac{\partial\omega_1}{\partial y_1^0}, \quad \frac{\partial\omega_1}{\partial y_2^0}, \quad \frac{\partial\omega_1}{\partial\beta}, \quad \frac{\partial\omega_2}{\partial y_1^0}, \quad \frac{\partial\omega_2}{\partial y_2^0}, \quad \frac{\partial\omega_2}{\partial\beta}. \tag{21}$$

As a specific example, we consider the rotation vector $\omega^0 = (\sqrt{2} - 1, \sqrt{3} - 1)$, and we fix $\alpha_1 = 0.1$ and $\alpha_2 = 0.2$. We ask for a tolerance of 10^{-23} in the computation of frequencies. If the error of the frequencies is larger than 10^{-20} after we reach the value $q_r = 20$, then we do not validate the results and we stop the computations. To perform the Newton method on the frequency map, we ask for a tolerance of 10^{-20} (i.e., we validate the results when the frequency map equals to ω^0 up to this tolerance). Results of this continuation are shown in the red curve of Fig. 1. The computation performs with significant accuracy (around 23 decimal digits for frequencies and 19 decimal digits for derivatives) up to $\beta \simeq 0.015$. Beyond this point, as we approach to the breakdown of the LIT, the width of the strip of analyticity of the parameterization shrinks. This loss of regularity affects the precision of the averaging-extrapolation methods. Anyway, we are still able to compute an initial condition on the LIT with at least 20 decimal digits up to the value $\beta \simeq 0.02778$. Although for larger values of β we cannot keep such level of accuracy, we still observe a nice and regular performance of the extrapolation methods in general and, particularly, in the computation of the derivatives. Accordingly, we expect the LIT to exist beyond the red curve. To carry out the continuation for $\beta > 0.02778$, we ask for a higher tolerance in the Newton method. Results of the continuation under less demanding tolerances are shown, using different colors, in Figs. 1 and 2. The information corresponding to the color scale is given in Table 1. We note that the accuracy of the derivatives (21) decreases as β approach to the last computed value $\beta \simeq 0.04189$. The asymptotic behavior of the size of these derivatives shows that this value is close to the blow up of the derivatives with respect to parameters. Hence, we are approaching to the breakdown of the LIT (see Table 2).

Table 1
Implementation parameters of the Newton method corresponding to the colored curves shown in Figs. 1 and 2. The rightmost column is the value of the parameter β for the last computed LIT in the curve.

Color	Tol. freq.	Tol. new.	Last computed β
Red	10^{-23}	10^{-20}	0.027781075132975380 2587
Green	10^{-21}	10^{-18}	0.032529941398995388 5507
Blue	10^{-18}	10^{-16}	0.037775451543391344838
Magenta	10^{-16}	10^{-14}	0.040896335210329690 0526
Black	10^{-14}	10^{-12}	0.041269962191088673 8677
Orange	10^{-12}	10^{-10}	0.041893321973131358 8506

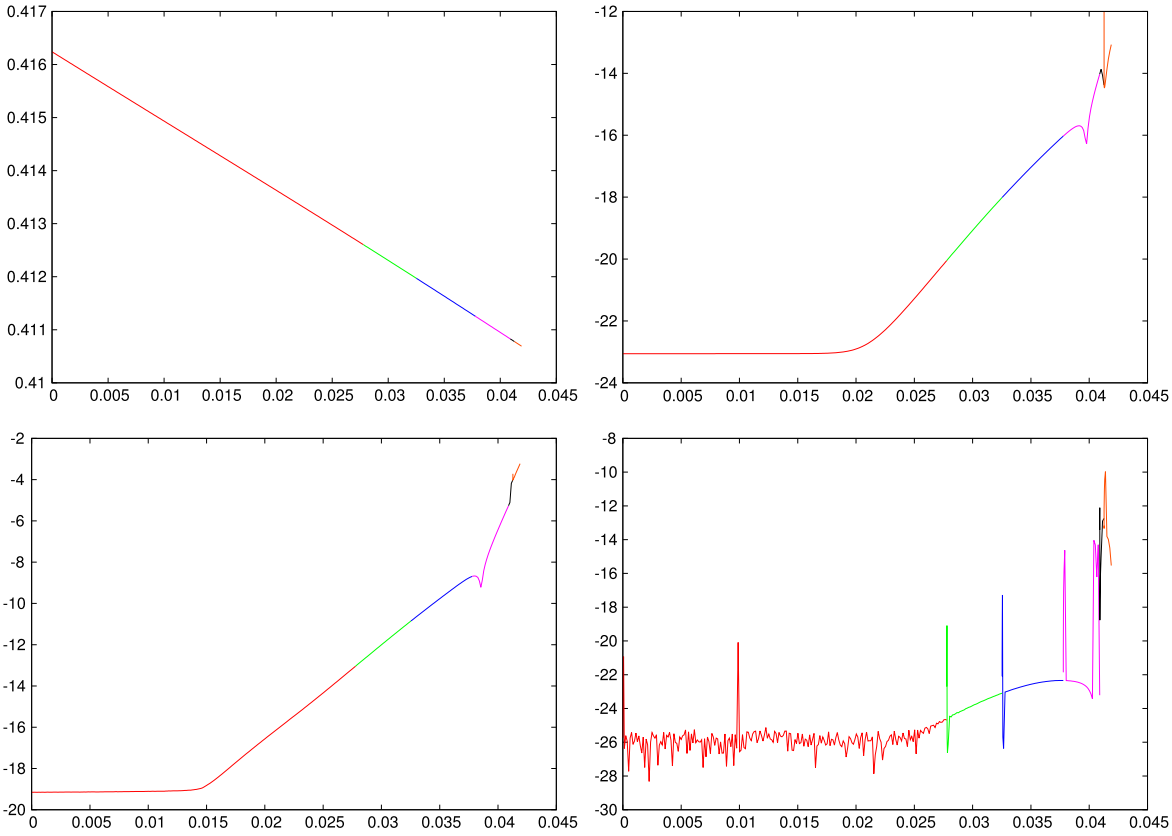

Fig. 1. Numerical continuation w.r.t. β (horizontal axis) of the LIT of rotation vector $(\omega_1^0, \omega_2^0) = (\sqrt{2}-1, \sqrt{3}-1)$ of (19) for $\alpha_1 = 0.1$, and $\alpha_2 = 0.2$. Colors correspond to the tolerance in the Newton method (see Table 1). Top-Left: initial condition y_1^0. Top-Right: $\log_{10}$ of the averaged extrapolation error in the computation of the two frequencies. Bottom-Left: $\log_{10}$ of the averaged extrapolation error in the computation of the six derivatives in (21). Bottom-Right: $\log_{10}$ of the error in the convergence of the Newton method.

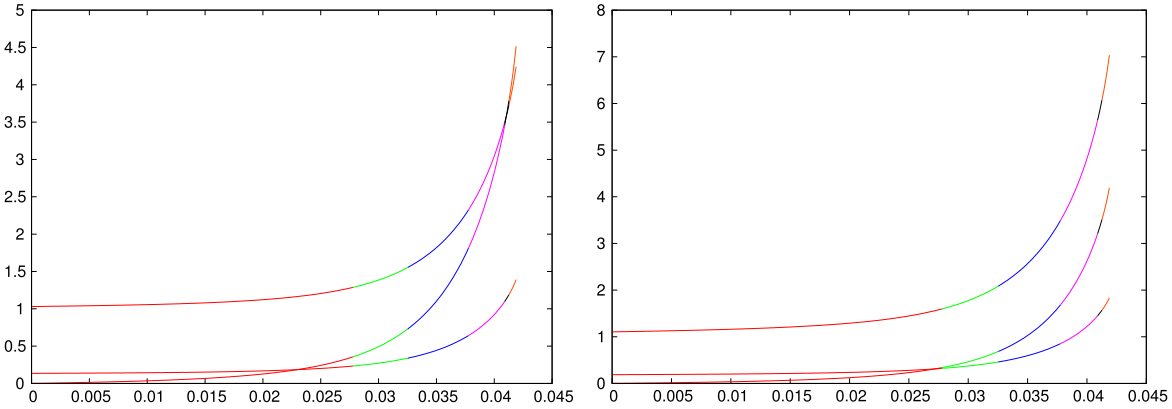

Fig. 2. Additional plots to the numerical continuation with respect to β of Fig. 1. Left: Absolute value of the derivatives of ω_1 with respect to (y_1^0, y_2^0, β). Right: Absolute value of the derivatives of ω_2 with respect to (y_1^0, y_2^0, β).

In order to illustrate the performance of the method when the dimension of the LIT (i.e., the number of frequencies) increases, we continue with respect to β a LIT of (19) for $r = 4$ and $r = 8$. Results for $r = 4$ are displayed in Table 3 and correspond to $\alpha_1 = 0.1$, $\alpha_2 = 0.2, \alpha_3 = 0.1, \alpha_4 = 0.2$, and rotation frequencies

$$\omega^0 = (\sqrt{2}-1, \sqrt{3}-1, \sqrt{5}-2, \sqrt{7}-2). \tag{22}$$

Results for $r = 8$ are displayed in Table 4 and correspond to $\alpha_i = 0.1, i = 1, \ldots, 8$, and

$$\omega^0 = (\sqrt{2}-1, \sqrt{3}-1, \sqrt{5}-2, \sqrt{7}-2, \sqrt{11}-3, \sqrt{13}-3, \sqrt{17}-4, \sqrt{19}-4). \tag{23}$$

If we focus on the lasts columns of Tables 3 and 4, we observe how the accuracy of the results is reduced as we approach to the breakdown of the LIT.

3.2. Study of a restricted three body problem

We consider two punctual masses (called primaries) describing an elliptic orbit, according to the Newton laws, with eccentricity e and semimajor axis a. The elliptic restricted three body problem (ERTBP) describes the motion of a third massless particle (an asteroid) under the gravitational attraction of the primaries. As usual, we consider a rotating coordinate system with origin at the center of mass of the primaries, so that the two primaries

Table 2
Some output data of the numerical continuation with respect to β of Figs. 1 and 2. In the last two columns we show the estimated error obtained for the frequencies in the Newton method.

β	y_1^0	y_2^0	$\lvert\omega_1-\omega_1^0\rvert$	$\lvert\omega_2-\omega_2^0\rvert$
9.7771691408155725462 7e−07	0.41623928063557881 8468	0.71797745492017305 3136	1e−26	2e−26
5.3808976756155030071 9e−03	0.41553521862139584 3133	0.71889001173336425 0169	2e−26	1e−25
1.1013753936711635224 2e−02	0.41480140523414110 5449	0.71984397601049617 3569	2e−27	2e−26
1.6896719831511736506 5e−02	0.41403554330471347 2584	0.72084218552549094 4118	2e−27	4e−26
2.2402781367250488745 7e−02	0.41331539178823931 4504	0.72178244310429966 4683	2e−26	1e−26
2.7781075132975380258 7e−02	0.41260450509383448 9587	0.72271120168541267 7265	1e−24	2e−24
2.9405394577880753830 2e−02	0.41238776016649650 1515	0.72299435665369098 7061	6e−24	8e−24
3.1530233170502158193 7e−02	0.41210261140110406 0735	0.72336681659859265 6407	3e−23	3e−23
3.3403600273832450431 1e−02	0.41184970108417318 9480	0.72369710838263253 5398	9e−23	1e−22
3.6526545079861178238 7e−02	0.41142530848608434 3014	0.72425127852083535 5351	2e−22	3e−22
3.8024242892721417041 6e−02	0.41122081660822621 3801	0.72451831646167026 6277	2e−22	3e−22
3.9397894689154336752 0e−02	0.41103290553537544 9688	0.72476374295528084 8283	1e−22	2e−22
4.0896335210329690052 6e−02	0.41082770871506235 0638	0.72503182178988660 3282	3e−23	5e−23

Table 3
Some output data of the numerical continuation with respect to β of the LIT of (19) of rotation frequencies (22) for $\alpha_1=\alpha_3=0.1$ and $\alpha_2=\alpha_4=0.2$. In the last column we show the sum of the estimated error obtained for the frequencies after the Newton method.

β	y_1^0	y_2^0	y_3^0	y_4^0	$\lvert\omega-\omega^0\rvert$
9.779439684885e−07	0.4162392678913	0.7179773739847	0.2447614664937	0.6381604610137	1e−25
1.242005127722e−04	0.4162214880000	0.7179880933506	0.2447554403886	0.6381754561794	4e−27
4.997557667751e−04	0.4161672921146	0.7180206035566	0.2447372441062	0.6382211619743	9e−27
6.317939443707e−04	0.4161482354020	0.7180319763522	0.2447309074316	0.6382372326375	3e−23
9.995637966472e−04	0.4160951491976	0.7180634968389	0.2447134243981	0.6382819984438	3e−17
1.625618649899e−03	0.4160047558418	0.7181166259178	0.2446842270968	0.6383582157448	5e−17
2.251751970294e−03	0.4159143181082	0.7181690986610	0.2446557367438	0.6384344580512	5e−17
2.751735327176e−03	0.4158420760031	0.7182105254825	0.2446334967205	0.6384953503886	3e−17
3.503267593603e−03	0.4157334427959	0.7182720067843	0.2446009199017	0.6385868964559	1e−16
4.254904463352e−03	0.4156247366839	0.7183325551101	0.2445693631055	0.6386784763119	9e−16
4.881346034123e−03	0.4155340898778	0.7183823029776	0.2445438461321	0.6387548179573	2e−15
5.383527613237e−03	0.4154613909064	0.7184217156897	0.2445239058184	0.6388160265805	1e−14
5.397232974486e−03	0.4154594064151	0.7184227855827	0.2445233679744	0.6388176971853	1e−12

Table 4
Some output data of the numerical continuation with respect to β of the LIT of (19) of rotation frequencies (23) for $\alpha_i=0.1$, $i=1,\ldots,8$. In the last column we show the sum of the estimated error obtained for the frequencies after the Newton method.

β	y_1^0 & y_5^0	y_2^0 & y_6^0	y_3^0 & y_7^0	y_4^0 & y_8^0	$\lvert\omega-\omega^0\rvert$
8.721026636145e−07	0.4162397440728	0.7249722133046	0.2447614773163	0.6419081663358	
	0.3217096059857	0.6029467432330	0.1431926686372	0.3625911181005	2e−23
6.104690229538e−06	0.4162417545974	0.7249725942790	0.2447612546689	0.6419086441563	
	0.3217089437365	0.6029470295899	0.1431922227900	0.3625892646069	5e−21
2.703455495136e−05	0.4162497977287	0.7249741172879	0.2447603646304	0.6419105550262	
	0.3217062949516	0.6029481748676	0.1431904395238	0.3625818498993	1e−18
1.107463501067e−04	0.4162819867430	0.7249801951158	0.2447568132825	0.6419181915871	
	0.3216957036192	0.6029527535822	0.1431833083655	0.3625521793992	3e−16
3.339203121380e−04	0.4163679521865	0.7249962918378	0.2447474116802	0.6419384941006	
	0.3216674995059	0.6029649448522	0.1431643056256	0.3624729682366	5e−15
5.570164172625e−04	0.4164541018311	0.7250122280960	0.2447381094064	0.6419586893359	
	0.3216393752779	0.6029771092797	0.1431453199186	0.3623936297754	4e−15
7.800418216508e−04	0.4165404330789	0.7250280047780	0.2447289057641	0.6419787550248	
	0.3216113592776	0.6029892471999	0.1431263476848	0.3623141682097	8e−15

are fixed on the x-axis, the z-axis has the direction of the angular momentum and the y-axis is defined to have a positive-oriented frame. If we choose units of distance, time, and mass such that $a=1$, the period is 2π and the sum of the masses is 1, and we take as independent variable the true anomaly f, then the Hamiltonian $H_e=H_e(x,y,z,p_x,p_y,p_z,f)$ for the third particle is 2π-periodic on f and is given by (e.g. [30])

$$H_e=\frac{(p_x+y)^2+(p_y-x)^2+p_z^2+z^2}{2}-\frac{1}{E}\left[\frac{x^2+y^2+z^2}{2}+\frac{1-\mu}{r_1}+\frac{\mu}{r_2}\right], \tag{24}$$

where $E=1+e\cos f$, $p_x=\dot{x}-y$, $p_y=\dot{y}+x$, $p_z=\dot{z}$, $r_1^2=(x-\mu)^2+y^2+z^2$, $r_2^2=(x-\mu+1)^2+y^2+z^2$, and $\mu\in(0,\frac{1}{2}]$ is the mass of the smallest primary. The connection between f and the time t is given by:

$$\dot{f}=(1-e^2)^{-3/2}(1+e\cos f)^2. \tag{25}$$

For $e=0$, we obtain the Circular Restricted Three Body Problem (CRTBP), given by the autonomous Hamiltonian

$$H_0(x,y,z,p_x,p_y,p_z)=\frac{p_x^2+p_y^2+p_z^2}{2}+yp_x-xp_y-\frac{1-\mu}{r_1}-\frac{\mu}{r_2}. \tag{26}$$

Although for $e\neq 0$ the Hamiltonian (24) is 2π-periodic, it has five equilibrium points. Three of them (the Eulerian points L_1, L_2, and L_3) are on the x axis, and the other two (the Lagrangian points L_4

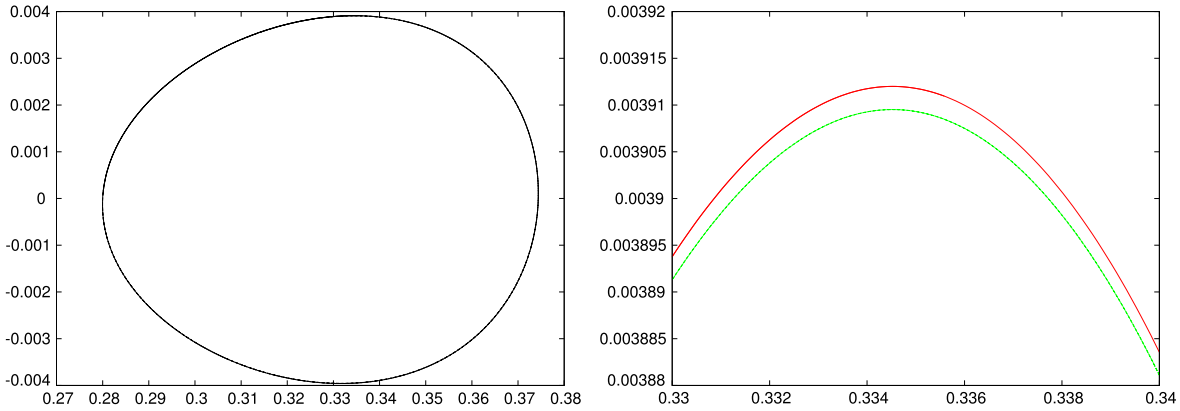

Fig. 3. Left: We show initial conditions α^0 (horizontal axis) versus ρ^0 (vertical axis) corresponding to the continuation of two families of LITs of the planar CRTBP, starting from (28) and satisfying $\omega_1 = \omega_1^0$ and $\omega_2 = \omega_2^0$, respectively (see (29)). Right: Zoom of the previous figure. The red curve corresponds to $\omega_1 = \omega_1^0$ and the green curve corresponds to $\omega_2 = \omega_2^0$. (For interpretation of the references to color in this figure legend, the reader is referred to the web version of this article.)

and L_5) are on the plane xy and form an equilateral triangle with the primaries. We focus on L_5 (the point L_4 is equivalent), given by $(\mu-\frac{1}{2}, \frac{\sqrt{3}}{2}, 0, -\frac{\sqrt{3}}{2}, -\frac{1}{2}+\mu, 0)$. It is well-known that for $e = 0$ and $0 < \mu < \mu_R$, where $\mu_R = \frac{1}{2}(1-\sqrt{23/27}) \simeq 0.03852$ is the Routh critical value, the point L_5 is linearly stable (elliptic) with normal frequencies

$$\omega_1^{(L_5)} = \left[\frac{1}{2}(1-(1-27\mu(1-\mu))^{1/2})\right]^{1/2}, \qquad \omega_2^{(L_5)} = \left[\frac{1}{2}(1+(1-27\mu(1-\mu))^{1/2})\right]^{1/2}, \tag{27}$$

and $\omega_3^{(L_5)} = 1$ (the one of the vertical oscillations).

In this section we use the Newton method on the frequency map to compute and continue numerically LITs around L_5 of the CRTBP and the ERTBP for the Sun–Jupiter system, given by $\mu_{SJ} = 0.00095388118$. KAM theory (e.g. [22,31]) predicts that there is a large set of LITs around L_5. For $e = 0$, the frequency analysis of the CRTBP for $\mu = \mu_{SJ}$ shows that L_5 is stable from the effective viewpoint (e.g. [20,19]) in a domain larger than the one for which the existence of LITs has been established (e.g. [32,20]).

In the computations performed below we consider initial conditions close to L_5 parameterized as follows:

$$x = \mu + (1+\rho)\cos(2\pi\alpha), \qquad y = (1+\rho)\sin(2\pi\alpha),$$
$$z = z, \qquad \dot{x} = \dot{y} = \dot{z} = 0, \qquad f = 0.$$

This selection of variables (α, ρ) is suitably adapted to the shape of the domain of stability of the problem. Taking zero velocity is a normalization condition for the LIT. Given an initial condition of this form, we assume that the corresponding trajectory belongs to a LIT of the system (with three frequencies for the CRTBP and four frequencies for the ERTBP). For $e \neq 0$ the time-frequency is known, so we focus on the remaining ones. For small values of e, these frequencies are close to the ones of L_5 for the CRTBP (see (27)). In particular, the motion restricted to the plane $z = 0$ has only two frequencies. We address the computation of the frequency map in terms of the complex signal $x_n + \mathrm{i}y_n - \Gamma$, where the values of x_n and y_n are defined by using sampling time $T = 1$. This implies that the frequencies of the discrete signal are the same as those of the continuous one. The value of Γ is an approximation to the average of the discrete signal, computed using with $p_f = 2$ and $q_f = 10$. Notice that removing the average of the signal is a useful trick to accelerate the convergence of the unfolding process. We use the extrapolation parameters $p_u = 2$ and $q_u = 10$ for the unfolding procedure and we use $p_r = 5$ and $q_r \leq 16$ for the computation of the frequencies and its derivatives. To integrate the Hamiltonian H_e we use a Taylor method of order 22 and double precision arithmetic.

3.2.1. The planar case

To illustrate the flexibility of our approach, we perform different continuations of LITs of the planar CRTBP following several criteria. As starting point, we consider the initial condition given by

$$\alpha = 0.28, \qquad \rho = 0, \qquad z = 0. \tag{28}$$

By performing frequency analysis of the corresponding trajectory (e.g. [19]) we obtain the frequencies

$$\omega_1^0/2\pi = 0.01258702486754, \qquad \omega_2^0/2\pi = 0.15861068715732. \tag{29}$$

To perform the computations, we ask for a tolerance of 10^{-14} in the computation of frequencies (but we do not explicitly control the accuracy of its derivatives) and a tolerance of 10^{-10} for the Newton method.

First, we continue LITs by fixing the value of one of the frequencies. Abusing notation, we denote by (ω_1, ω_2) the components of the frequency map as function of the initial values ρ^0 and α^0. Then, the considered equations are $\omega_1 = \omega_1^0$ and $\omega_2 = \omega_2^0$. Each of these equations defines a curve on the plane $\alpha^0\rho^0$. Note that there is a dense set of resonances as the other frequency moves along the curve. However, since no low-order resonances are encountered, we do not observe these holes numerically. Both curves are shown in the left plot of Fig. 3 and they define a convex domain around the point $(\alpha^0, \rho^0) = (1/3, 0)$, that corresponds to L_5. These curves are very close to each other. In the right plot in Fig. 3 we display a zoom to show that they are different. This close-to-degenerate behavior is typically observed in celestial mechanics, since it is common that frequencies move very slowly with respect to initial conditions.

Next, we deal with the iso-energetic continuation $\omega_2/\omega_1 = \omega_2^0/\omega_1^0$ using the energy $E = H_0$ as a parameter. Now, we obtain a continuous curve very similar to the left plot of Fig. 3. In the same way, the value of λ defined by $(\omega_1, \omega_2) = \lambda \cdot (\omega_1^0, \omega_2^0)$ remains close to 1. Some points of the continuation are given in Table 5.

Finally, we consider the initial conditions of two different LITs of the planar CRTBP, and we use the method of Section 2.4 to compute some Fourier coefficients of the corresponding parameterizations. In this way, we illustrate that we can obtain a good enough approximation of the parameterization with a reasonable computational cost. As noted in Section 2.4, this approximate parameterization an be introduced as an initial guess for a parameterization KAM method. Explicitly, we consider the LITs with initial conditions given by (28) and the gray row in Table 5. In both cases the corresponding frequencies are known. Then, we take $p_f = 7$ and $q_f = 18$, and we compute $\hat{\gamma}_k$, $k =$

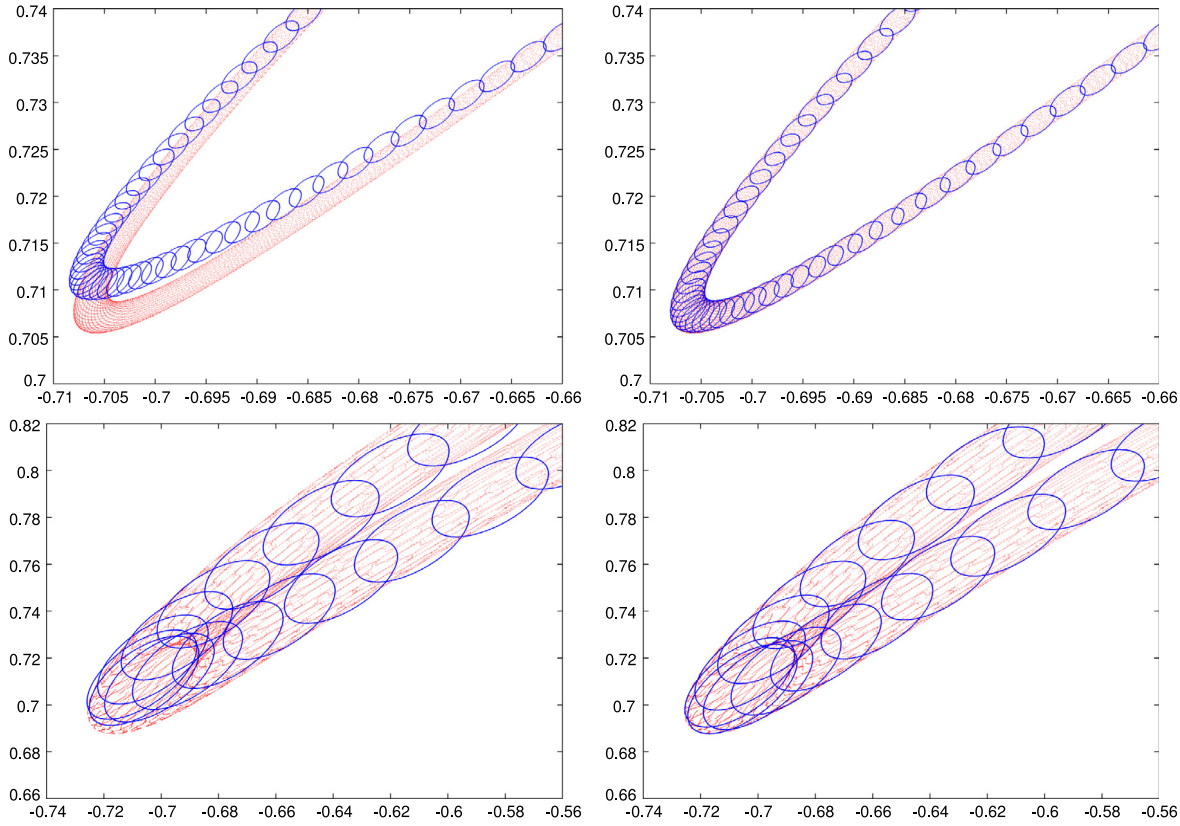

Fig. 4. We compare in the plane xy the numerical integration of a trajectory on a LIT of the CRTBP with an approximate parameterization of the LIT. Top plots correspond to the LIT with initial condition (28) and bottom plots correspond to initial condition in the gray row of Table 5. Left plots correspond to the truncated parameterization defined by the Fourier coefficients of order $k = (k_1, k_2)$ for $|k_1| + |k_2| \leq 3$, $|k_1| \leq 2$, and $|k_2| \leq 2$. Right plots correspond to the Fourier coefficients for $|k_1| + |k_2| \leq 5$, $|k_1| \leq 4$, and $|k_2| \leq 4$. (For interpretation of the references to color in this figure legend, the reader is referred to the web version of this article.)

Table 5
A list of initial conditions on corresponding to iso-energetic continuation of the initial condition (28) for the planar CRTBP.

α^0	ρ^0	ω_1	ω_2	E
0.280192522668237	−4.746451733802e−04	1.258701184120e−02	1.586106869295e−01	−1.499615628007
0.283551429742507	−1.467835855603e−03	1.258701153345e−02	1.586106830516e−01	−1.499608162928
0.291387651385253	−2.442251747710e−03	1.258701087304e−02	1.586106747299e−01	−1.499592054697
0.312418101104665	−3.641388980651e−03	1.258700955220e−02	1.586106580907e−01	−1.499559474274
0.349860839393634	−3.620165867824e−03	1.258700942856e−02	1.586106565275e−01	−1.499556387157
0.369186023210945	−1.920472002072e−03	1.258701108022e−02	1.586106773404e−01	−1.499597121045
0.373886557767825	−5.446218663226e−04	1.258701174412e−02	1.586106857269e−01	−1.499613316143
0.373639891395473	9.059898423750e−04	1.258701170747e−02	1.586106852443e−01	−1.499612387125
0.371338111569159	1.670287803542e−03	1.258701136790e−02	1.586106809653e−01	−1.499604135924
0.364930005843379	2.685801790546e−03	1.258701056931e−02	1.586106709022e−01	−1.499584604355
0.346262823927619	3.774163590467e−03	1.258700925423e−02	1.586106543306e−01	−1.499552041160
0.337949663115750	3.901040603424e−03	1.258700905388e−02	1.586106518137e−01	−1.499547050923
0.301019986433853	2.946177436291e−03	1.258701016835e−02	1.586106658496e−01	−1.499574729371
0.281997822713248	8.833214227426e−04	1.258701167269e−02	1.586106848164e−01	−1.499611563592

(k_1, k_2), for $|k_1| + |k_2| \leq 5$, $|k_1| \leq 4$, and $|k_2| \leq 4$. Results are shown in Fig. 4. We show in red some points corresponding to the numerical integration of the initial condition. In blue, we plot some curves obtained by mapping by the approximated parameterization some circles of the form $\theta_1 = \text{const.}$ and $\theta_2 = \text{const.}$ In both cases we observe a very nice agreement between the blue and red figures.

3.2.2. The spatial case

If $e = 0$, we cannot properly speak about the stability domain of L_5 in the spatial CRTBP, as the 3-dimensional LITs of the system do not act as barriers in the 5-dimensional energy manifolds. The same happens if $e \neq 0$, since we have 4-dimensional LITs in the 7-dimensional extended phase space. Hence, for a general trajectory of these spatial problems, we can only ask for effective stability (i.e., stability for a very long time span). Nevertheless, the domain of effective stability of the spatial CRTBP behaves similarly as the domain of perpetual stability in the planar CRTBP. We refer to [19] for a complete frequency analysis of this domain.

First, we perform the numerical continuation of 3-dimensional LITs in the spatial CRTBP. We consider the LIT of the planar CRTBP with initial condition given in (28) and frequencies ω_1^0 and ω_2^0 given in (29). If we denote by $\mathcal{F} = (\omega_1, \omega_2, \omega_3)$ the frequency map of the spatial CRTBP, defined as function of the variables (α, ρ, z), labeling the selected initial conditions, then the equations $\omega_1 = \omega_1^0$ and $\omega_2 = \omega_2^0$ define a Cantor curve in the (α, ρ, z)-space, that we parameterize by the arc parameter. The vertical frequency ω_3 moves along this curve, close to the initial value $\omega_3^0 = 1$. We ask for a tolerance of 10^{-14} in the computation of the frequencies and 10^{-10} in the Newton method. Results are shown in the left plot of

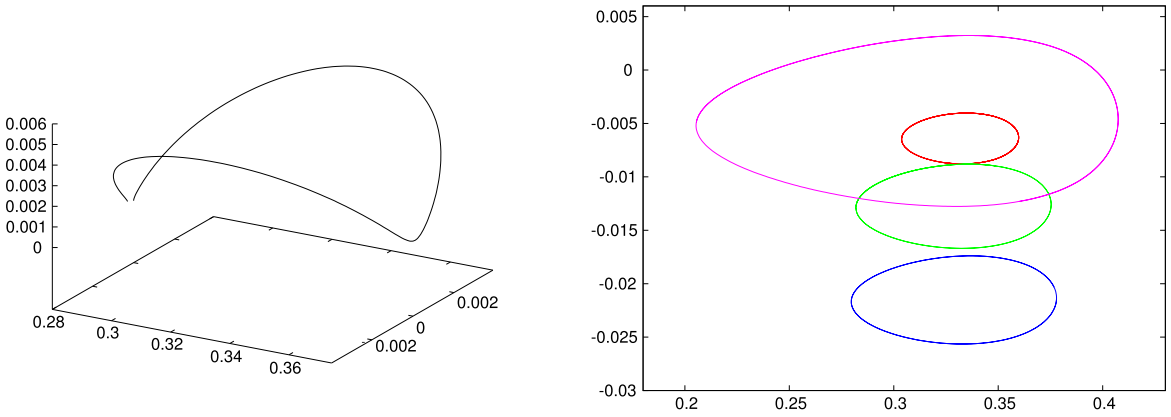

Fig. 5. Numerical continuation of LITs in the spatial CRTBP defined by $\omega_1 = \omega_1^0$ and $\omega_2 = \omega_2^0$, for different values of ω_1^0 and ω_2^0. Left: We show the continuation curve in the (α, ρ, z)-space, for $z > 0$, for the frequencies (29). Right: We show the (ρ, α)-projection of the continuation curve for the initial conditions given by (30) (in red), (31) (in green), (32) (in blue), and (33) (in magenta).

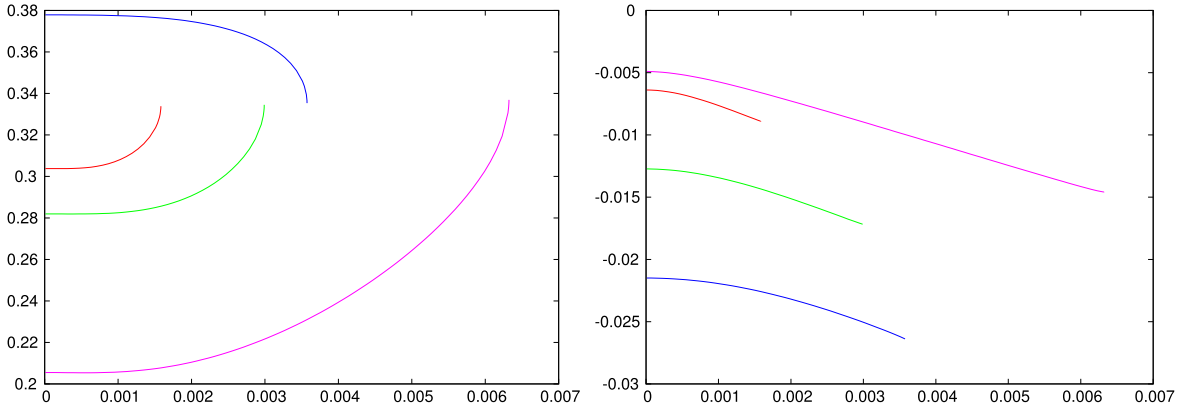

Fig. 6. Numerical continuation of LIT in the spatial ERTBP with respect to e, defined by the equations $\omega_1 = \omega_1^0$, $\omega_2 = \omega_2^0$ and $\omega_3 = \omega_3^0$, for the values of ω_1^0, ω_2^0 and ω_3^0 associated to the initial conditions given by (30) (in red), (31) (in green), (32) (in blue), and (33) (in magenta). Left: We show the parameter α vs e. Right: We show the parameter ρ vs e. (For interpretation of the references to color in this figure legend, the reader is referred to the web version of this article.)

Fig. 5. We perform similar computations starting from other four spatial LITs close to L_5, which are characterized by the following initial conditions

$$\alpha = 0.30378, \quad \rho = -0.0063897277308054, \quad z = 0.16, \quad (30)$$
$$\alpha = 0.28194, \quad \rho = -0.0127279858304461, \quad z = 0.226, \quad (31)$$
$$\alpha = 0.37788, \quad \rho = -0.0214910665205657, \quad z = 0.294, \quad (32)$$
$$\alpha = 0.20550, \quad \rho = -0.0048939829652115, \quad z = 0.14. \quad (33)$$

These LITs have "planar frequencies" given, respectively, by

$$\omega_1^0/2\pi = 0.0126239732852498,$$
$$\omega_2^0/2\pi = 0.158641602983746;$$
$$\omega_1^0/2\pi = 0.0123864185088543,$$
$$\omega_2^0/2\pi = 0.158640812829964;$$
$$\omega_1^0/2\pi = 0.0122301409937443,$$
$$\omega_2^0/2\pi = 0.158658687002319;$$
$$\omega_1^0/2\pi = 0.0116130461983901,$$
$$\omega_2^0/2\pi = 0.158552760666373.$$

These frequencies have been computed by frequency analysis (see [19]). The corresponding continued families of LITs associated to the equations $\omega_1 = \omega_1^0$ and $\omega_2 = \omega_2^0$ are shown in the right plot of Fig. 5.

The final application is the numerical continuation of LITs in the (spatial) ERTBP. If we denote the frequency map of H_e as $\omega = (\omega_1, \omega_2, \omega_3, \omega_4)$, then ω_4 takes the constant value $\omega_4 = 1$. Hence, we only need three parameters to characterize a LIT of H_e, so we can use the variables (α, ρ, z) that parameterize the selected initial conditions on the zero velocity manifold having zero true anomaly. For any initial parameters (α^0, ρ^0, z^0) labeling an invariant torus of the spatial CRTBP (for $e = 0$), with frequency vector $(\omega_1^0, \omega_2^0, \omega_3^0)$, we continue numerically with respect to e the LIT that verifies $\omega_1 = \omega_1^0$, $\omega_2 = \omega_2^0$, and $\omega_3 = \omega_3^0$. If the vector $(\omega_1^0, \omega_2^0, \omega_3^0, \omega_4^0 = 1)$ is Diophantine, then the continuation curve is continuous in the (α, ρ, z)-space. We illustrate this process considering the four initial conditions given by (30)–(33). The third frequency associated to these initial conditions is given by $\omega_3^0/2\pi = 0.159157707621790$, $\omega_3^0/2\pi = 0.159162876109802$, $\omega_3^0/2\pi = 0.159162723016639$, and $\omega_3^0/2\pi = 0.159195170134776$, respectively. The result of this numerical continuation is shown in Fig. 6. We stop the computations at the turning point that appears for $\alpha \simeq 1/3$, that is, when the LIT is situated above the point L_5. It is worth mentioning that this is not a destruction mechanism of LITs. This simply means that we cannot expect to find LITs of a given frequency vector for arbitrary values of the eccentricity. We point out that the larger value of the eccentricity that we obtain for the selected LITs is $e \simeq 0.0063$, which is far away from the actual value of the eccentricity of the Sun–Jupiter system, $e_{SJ} = 0.048775$. This occurs because the values attained by the frequency map around the point L_5 change significantly when we move e. Hence, even for significantly small values of e, we cannot expect to find a LIT of H_e with the same frequencies as for the case $e = 0$. For example, a frequency analysis

reveals that, for $e = e_{SJ}$, the frequencies around L_5 are $\omega_1 \simeq 0.0129$ and $\omega_2 \simeq 0.15784$.

Acknowledgments

We want to thank Arturo Vieiro for many discussions and comments. Some of these discussions led to interesting ideas that will be presented in a subsequent work. We also want to thank the anonymous referee for valuable suggestions that considerably improved the quality of the manuscript.

References

[1] H.W. Broer, G.B. Huitema, M.B. Sevryuk, Quasi-periodic motions in families of dynamical systems. Order amidst chaos, in: Lecture Notes in Math., vol. 1645, Springer-Verlag, Berlin, 1996.
[2] R. de la Llave, A tutorial on KAM theory, in: Smooth Ergodic Theory and its Applications (Seattle, WA, 1999), in: Proc. Sympos. Pure Math., vol. 69, Amer. Math. Soc., Providence, RI, 2001, pp. 175–292.
[3] À. Haro, M. Canadell, J.-Ll. Figueras, A. Luque, J.M. Mondelo, The parameterization method for invariant manifolds: from theory to effective computations, Manuscript.
[4] F. Schilder, H.M. Osinga, W. Vogt, Continuation of quasi-periodic invariant tori, SIAM J. Appl. Dyn. Syst. 4 (3) (2005) 459–488. (electronic).
[5] F. Gabern, À. Jorba, U. Locatelli, On the construction of the Kolmogorov normal form for the Trojan asteroids, Nonlinearity 18 (4) (2005) 1705–1734.
[6] G. Gómez, À. Jorba, J. Masdemont, C. Simó, Study of Poincaré maps for orbits near Lagrangian points. ESA-ESOC contract 8711/91/D/IM/(SC), Darmstadt, Germany, 1993.
[7] À. Jorba, J. Villanueva, Numerical computation of normal forms around some periodic orbits of the restricted three-body problem, Physica D 114 (3–4) (1998) 197–229.
[8] C. Simó, Effective computations in celestial mechanics and astrodynamics, in: Modern Methods of Analytical Mechanics and their Applications (Udine, 1997), Springer, Vienna, 1998, pp. 55–102.
[9] L. Dieci, J. Lorenz, R.D. Russell, Numerical calculation of invariant tori, SIAM J. Sci. Stat. Comput. 12 (3) (1991) 607–647.
[10] E. Castellà, À. Jorba, On the vertical families of two-dimensional tori near the triangular points of the bicircular problem, Celestial Mech. Dynam. Astronom. 76 (1) (2000) 35–54.
[11] M. Huang, T. Küpper, N. Masbaum, Computation of invariant tori by the Fourier methods, SIAM J. Sci. Comput. 18 (3) (1997) 918–942.
[12] F. Schilder, H.M. Osinga, W. Vogt, Fourier methods for quasi-periodic oscillations, Internat. J. Numer. Methods Engrg. 67 (5) (2006) 629–671.
[13] G. Huguet, R. de la Llave, Y. Sire, Computation of whiskered invariant tori and their associated manifolds: new fast algorithms, Discrete Contin. Dyn. Syst. 32 (4) (2012) 1309–1353.
[14] R. de la Llave, A. González, À. Jorba, J. Villanueva, KAM theory without action-angle variables, Nonlinearity 18 (2) (2005) 855–895.
[15] Chr. Kaas-Petersen, Computation, continuation, and bifurcation of torus solutions for dissipative maps and ordinary differential equations, Physica D 25 (1–3) (1987) 288–306.
[16] T.M. Seara, J. Villanueva, On the numerical computation of Diophantine rotation numbers of analytic circle maps, Physica D 217 (2) (2006) 107–120.
[17] A. Luque, J. Villanueva, Computation of derivatives of the rotation number for parametric families of circle diffeomorphisms, Physica D 237 (20) (2008) 2599–2615.
[18] A. Luque, J. Villanueva, Numerical computation of rotation numbers for quasi-periodic planar curves, Physica D 238 (20) (2009) 2025–2044.
[19] A. Luque, J. Villanueva, Quasi-periodic frequency analysis using averaging-extrapolation methods, SIAM J. Appl. Dyn. Syst. 13 (1) (2014) 1–46.
[20] G. Gómez, J.-M. Mondelo, C. Simó, A collocation method for the numerical Fourier analysis of quasi-periodic functions. I. Numerical tests and examples, Discrete Contin. Dyn. Syst. Ser. B 14 (1) (2010) 41–74.
[21] J. Laskar, The chaotic motion of the solar system. A numerical estimate of the size of the chaotic zones, Icarus 88 (1990) 266–291.
[22] À. Jorba, J. Villanueva, On the normal behaviour of partially elliptic lower-dimensional tori of Hamiltonian systems, Nonlinearity 10 (4) (1997) 783–822.
[23] S. Das, Y. Saiki, E. Sander, J.A. Yorke, Quantitative quasiperiodicity, Preprint available at arXiv, num: arXiv:1508.00062.
[24] A. Luque, A. Vieiro, Jet transport in frequency analysis, in preparation.
[25] G. Benettin, L. Galgani, A. Giorgilli, Numerical investigations on a chain of weakly coupled rotators in the light of classical perturbation theory, Nuovo Cimento B (11) 89 (2) (1985) 103–119.
[26] A. Haro, R. de la Llave, New mechanisms for lack of equipartition of energy, Phys. Rev. Lett. 85 (9) (2000) 1859–1862.
[27] E. Fermi, J. Pasta, S. Ulam, M. Tsingou, Studies of Nonlinear Problems I. Technical Report LA 1940, Los Alamos Scientific Laboratory, 1955.
[28] B.V. Chirikov, A universal instability of many-dimensional oscillator systems, Phys. Rep. 52 (5) (1979) 264–379.
[29] C. Froeschlé, Numerical study of a four-dimensional mapping, Astron. Astrophys. 16 (1972) 172–189.
[30] V. Szebehely, Theory of Orbits — The Restricted Problem of Three Bodies, Academic Press, New York, 1967.
[31] À. Jorba, J. Villanueva, On the persistence of lower-dimensional invariant tori under quasi-periodic perturbations, J. Nonlinear Sci. 7 (5) (1997) 427–473.
[32] A. Celletti, A. Giorgilli, On the stability of the Lagrangian points in the spatial restricted problem of three bodies, Celestial Mech. Dynam. Astronom. 50 (1) (1991) 31–58.